"Study of Temperature Anisotropy and Kappa Distribution Impacts on EMIC Waves in Multi-Species Magnetized Plasma"

Rahul Bhaisaniya[1] and Ganpat Ahirwar[2]

[1]Assistant Professor,Govt PG college Rajgarh, MP,India

[2]Assistant Professor ,School of Studies in Physics,Vikram University Ujjain (M.P.)India

Correspondence: RAHUL BHAISANIYA (rahulbhaisaniya@gmail.com)

Abstract:- This research investigates the impact of temperature anisotropy on Electromagnetic ion cyclotron (EMIC) waves in a multi-ion magneto-plasma environment composed of H^+, He^+, and O^+ ions, with a particular emphasis on the role of the Kappa distribution function. The study delves into how variations in temperature anisotropy influence the behavior and properties of EMIC wave propagation, considering the complex interplay between anisotropic thermal effects and the non-Maxwellian Kappa distribution. Through a comprehensive analysis involving theoretical modeling and numerical simulations, the research elucidates how these factors alter wave dispersion relations, growth rates, and spatial structures of EMIC waves. The results reveal significant deviations from classical Maxwellian predictions, highlighting the necessity to incorporate Kappa distributions for accurate descriptions of wave behavior in realistic plasma conditions. This enhanced understanding has broader implications for space physics, astrophysical phenomena, and laboratory plasma experiments, where non-equilibrium conditions and multiple ion species are prevalent. The results are analyzed in the context of space plasma parameters relevant region within Earth's magnetosphere.

1. Introduction

EMIC waves are transverse, low-frequency (below the proton cyclotron frequency) waves typically in the range of 0.1–5 Hz, which manifest as Pc1–Pc2 pulsations on the ground. These waves are primarily generated in the equatorial region of Earth's magnetosphere and propagate along magnetic field lines as left-handed, circularly polarized waves, guided toward the ionosphere (Sugiyama et al., 20151999). Their oblique propagation characteristics and interactions with anisotropic plasma distributions have been extensively studied (Cattaert, et al., , Hellberg & Mace, 2007). Experimental evidence for naturally occurring ion cyclotron instabilities has been comprehensively summarized by Cornwall (1965).

In the auroral acceleration region, located at magnetic latitudes of approximately ±70° and altitudes above 4000 km, large-amplitude electric field structures have been observed. The parallel electric fields in this region, concentrated around 6000 km altitude, are strongly associated with field-aligned

currents (Yan et al., 2008). This region is characterized by low plasma beta (β) and cold plasma environments, making it a critical zone for understanding wave-particle interactions. EMIC waves play a vital role in space plasma physics, particularly in the Earth's magnetosphere, where they influence particle dynamics, energy transfer, and plasma stability (Gary & Lee , 1994). These waves interact with energetic particles, drive pitch-angle scattering, and facilitate the heating of ion populations, making them a cornerstone of magnetospheric studies (Kennel & Petschek, 1966; Chen & Hasegawa, 1974). The triggered emissions associated with EMIC waves have been observed in satellite data and analyzed in theoretical studies (Omura et al., 2010).

The propagation of EMIC waves at frequencies near the ion cyclotron frequency has been extensively studied under the assumption of Maxwellian velocity distributions, which describe thermal plasmas. However, real plasma environments, especially in the magnetosphere, often deviate from thermal equilibrium due to the presence of suprathermal particles (Sugiyama et al., 2015). The Kappa distribution function (Vasyliunas, 1968) is widely used to describe such non-thermal plasma environments. It is characterized by the parameter , which governs the extent of high-energy tails in the particle velocity distribution. Lower kappa values correspond to stronger deviations from thermal equilibrium, making the Kappa distribution particularly relevant for modeling space plasmas where suprathermal particles dominate (Pierrard & Lazar, 2010). A generalized plasma dispersion function for kappa-Maxwellian velocity distributions has been formulated to describe the wave behavior in these conditions (Hellberg & Mace, 2002).

Temperature anisotropy, where the temperature differs along directions parallel and perpendicular to the magnetic field, further adds complexity to the plasma environment. This anisotropy significantly influences wave growth, dispersion characteristics, and stability. In anisotropic magneto-plasma, enhanced perpendicular temperatures relative to the parallel component can amplify EMIC wave growth and alter dispersion relations compared to isotropic conditions (Hellinger & Matsumoto, 2000). When coupled with the Kappa distribution, temperature anisotropy introduces novel wave behaviors and complexities that deviate significantly from Maxwellian models (Lazar et al., 2006). The effects of temperature anisotropy on wave growth have been observed in bi-Kappa distributed plasmas, where deviations from Maxwellian distributions further modify wave dispersion (Lazar, 2012). The influence of suprathermal protons on EMIC wave instability thresholds has also been examined in kappa-distributed plasmas (Xiao et al., 2007).

Despite extensive research on plasma instabilities, a significant gap remains in understanding how temperature anisotropy and Kappa distributions simultaneously affect EMIC wave dynamics. The novelty of this study lies in addressing this critical gap by examining how temperature anisotropy influences the dispersion relations, growth rates, and spatial structures of EMIC waves in a multi-ion

magneto-plasma under the influence of the Kappa distribution. Unlike earlier works that focused predominantly on single-ion plasmas or isotropic temperature assumptions, this research emphasizes the role of multi-ion plasma composition (e.g., H^+, He^+, O^+) and varying kappa values, which are particularly relevant for understanding wave-particle interactions near the plasmapause and auroral acceleration regions. Previous studies have demonstrated how EMIC waves grow and dampen under different conditions, including oblique propagation and multi-ion species effects (Xue et al., Thorne, & Summers, 1996a, 1996b).

This study investigates the combined effects of temperature anisotropy and the Kappa distribution on EMIC wave dynamics, focusing on perpendicular and parallel resonant energies, growth rate, and growth length in a multi-ion plasma environment. By incorporating these complex plasma conditions, we aim to advance the accuracy of space plasma models, particularly within the magnetosphere, where these factors are paramount. The findings hold significant implications for space weather forecasting and the mitigation of associated disturbances, given EMIC waves influence on particle precipitation, ion heating, and geomagnetic activity. By rigorously quantifying the individual and combined impact of the Kappa distribution and temperature anisotropy, this research provides deeper insights into EMIC wave behaviour, enhancing our understanding of wave-particle interactions in space plasmas thereby improving the interpretation of satellite data.

2. Basic trajectories

Considering the trajectory of a charged particle in the presence of EMIC waves, various properties have been derived for different Kappa distribution indices (RanaMeda et al., 2021). Given that the wave propagates along the z-axis in the direction of the background magnetic field, the left-handed circularly polarized EMIC wave in a cold magnetized plasma with angular frequency ω can be expressed as follows:

$$B_x = \cos(k_{\varPi}z - \omega t) \tag{1}$$

$$B_y = \sin(k_{\varPi}z - \omega t) \tag{2}$$

When the system moves with the wave, the electric field reduces to zero. The total wave magnetic field is:

$$B = B_x \cos(k_{\varPi}z)\, x + B_y \sin(k_{\varPi}z)\, y \tag{3}$$

where

B: Wave magnetic field amplitude. $k_{\varPi}$: Wave number along the z-axis. ω : Angular frequency.

In the wave frame, moving with phase velocity , the position and velocity transformations are:

98 Where the following conditions apply (~~Rana~~Meda et al., 2021)

$$Z^{wave} = Z^{lab} - \left(\frac{\omega}{k_{\Pi l}}\right) t \tag{4}$$

$$V^{wave} = V^{lab} - \left(\frac{\omega}{k}\right) t \tag{5}$$

101 As $\frac{ck}{\omega} \gg 1$, As   The magnetic field amplitude is considered identical. Z^{wave}: Position of the particle
102 in the wave frame of reference.

103 V^{wave}: Position of the particle in the laboratory frame of reference. Thus, the equation of ion motion
104 in the wave is given as

$$\frac{dv_l}{dt} = \frac{q_l}{m_l c}[(V_l \times B_O) + (V_l \times B)] \tag{6}$$

106 q_l: Ion charge , m_l: Ion mass, c: Speed of light, B_O: Background magnetic field, B :Wave magnetic
107 field.

108 We use cylindrical coordinates in velocity space as follows

$$v_{lx} = V_{\perp l} \cos\phi \tag{7}$$

$$v_{ly} = V_{\perp l} \sin\phi \tag{8}$$

$$v_{\perp lz} = V_{\Pi l} \tag{9}$$

112 Where $V_{\perp l}$: Perpendicular velocity magnitude, $V_{\Pi l}$: Parallel velocity, ϕ: Gyrophase angle. Π:means
113 parallel to the magnetic field it refers to the component of velocity along the background magnetic
114 field direction. ~~The equation of motion is written as~~ The perpendicular component of the equation of
115 motion is:

$$\frac{dV_{\perp l}}{dt} = -V_{\Pi l}\Omega_l \sin(k_{\Pi}z - \phi) \tag{10}$$

$$V_{\perp l} = V_{\Pi l o} + \delta V_{\perp l} \tag{11}$$

$$V_{\Pi l} = V_{\Pi l o} + \delta V_{\Pi l} \tag{12}$$

119 Where V $_{\Pi i}$ initial values at t=0, Substituting eq. (1) to (5) in eq. (11) and (12) we find the following
120 the perturbations in perpendicular and parallel velocities due to the EMIC wave are: ~~equations of The~~
121 ~~alterations in multi-ion velocities in the context of an EMIC wave are provided as~~ (~~Rana~~Meda et al.,
122 2021)

123 $\delta V_{\perp l} = \frac{\left[h\Omega_{H^+}\left(V_{\Pi H^+} - \frac{\omega}{K_\Pi}\right)\right]}{[k_\Pi V_{\Pi H^+o} - (\omega - \Omega_{H^+})]} \times [\cos(k_{\Pi l}z - \omega t - \Psi) - \varepsilon \cos(k_{\Pi l}z - \omega t - \Psi - (k_{\Pi l}V_{\Pi H^+o} - $

124 $(\omega - \Omega_{H^+}))t] + \frac{\left[h\Omega_{He^+}\left(V_{\Pi He^+} - \frac{\omega}{K_\Pi}\right)\right]}{[k_\Pi V_{\Pi He^+o} - (\omega - \Omega_{He^+})]} \times [\cos(k_{\Pi l}z - \omega t - \Psi) - \varepsilon \cos(k_{\Pi l}z - \omega t - \Psi - $

125 $(k_{\Pi l}V_{\Pi He^+o} - (\omega - \Omega_{He^+}))t] + \frac{\left[h\Omega_{O^+}\left(V_{\Pi O^+} - \frac{\omega}{K_\Pi}\right)\right]}{[k_\Pi V_{\Pi O^+o} - (\omega - \Omega_{O^+})]} \times [\cos(k_{\Pi l}z - \omega t - \Psi) - \varepsilon \cos(k_{\Pi l}z - \omega t - $

126 $\Psi - (k_{\Pi l}V_{\Pi O^+o} - (\omega - \Omega_{O^+}))t]$ (13)

127 $\delta V_{\Pi l} = \frac{-hV_{\perp o}\Omega_{H^+}}{[k_\Pi V_{\Pi H^+o} - (\omega - \Omega_{H^+})]} \times [\cos(k_\Pi z - \omega t - \Psi) - \varepsilon \cos(k_\Pi z - \omega t - \Psi - (k_\Pi V_{\Pi H^+o} - (\omega - $

128 $\Omega_l))t] + \frac{-hV_{\perp o}\Omega_{H^+}}{[k_\Pi V_{\Pi He^+o} - (\omega - \Omega_{He^+})]} \times [\cos(k_\Pi z - \omega t - \Psi) - \varepsilon \cos(k_\Pi z - \omega t - \Psi - (k_\Pi V_{\Pi He^+o} - $

129 $(\omega - \Omega_l))t] + \frac{-hV_{\perp o}\Omega_{O^+}}{[k_\Pi V_{\Pi O^+o} - (\omega - \Omega_{O^+})]} \times [\cos(k_\Pi z - \omega t - \Psi) - \varepsilon \cos(k_\Pi z - \omega t - \Psi - (k_\Pi V_{\Pi O^+o} - $

130 $(\omega - \Omega_l))t]$ (14)

131 Where $z = z_0 + V_\Pi t$ and $\psi = \psi_0 - \omega t$ and where ε=0 for non-resonant particles and ε=1 for

—

132 resonant particles $h = \frac{B}{B_0}$. where $l = H^+/He^+/O^+$.

3. Distribution function

134 To examine *r*esonant and *non-r*esonant energies, growth rates, and growth lengths, we apply a Kappa

135 distribution function as an extension within a multi-ion magneto-plasma environment of previous work

136 (~~Rana~~Meda et al., 2021, Livadiotis, 2017 , Summers, & Thorne, 1991)

137 $F_k(V_l) = \frac{1}{\pi^{3/2}} \frac{1}{V_{\perp H^+}^2 + V_{\Pi H^+}^2} \frac{\Gamma(k_p+1)}{k_p{}^{3/2}\Gamma(k_p-1/2)} \times \left\{1 + \frac{V_{\Pi H^+}^2}{k_p V_{\perp H^+}^2} + \frac{V_{\perp H^+}^2}{k_p V_{T\perp H^+}^2}\right\}^{-k_p-1} + $

138 $\frac{1}{\pi^{3/2}} \frac{1}{V_{\perp He^+}^2 + V_{\Pi He^+}^2} \frac{\Gamma(k_p+1)}{k_p{}^{3/2}\Gamma(k_p-1/2)} \times \left\{1 + \frac{V_{\Pi He^+}^2}{k_p V_{\perp He^+}^2} + \frac{V_{\perp He^+}^2}{k_p V_{T\perp He^+}^2}\right\}^{-k_p-1} + \frac{1}{\pi^{3/2}} \frac{1}{V_{\perp O}^2 + V_{\Pi O^+}^2} \frac{\Gamma(k_p+1)}{k_p{}^{3/2}\Gamma(k_p-1/2)} \times$

139 $\left\{1 + \frac{V_{\Pi O^+}^2}{k_p V_{\perp O^+}^2} + \frac{V_{\perp O^+}^2}{k_p V_{T\perp O^+}^2}\right\}^{-k_p-1}$ (15)

140 $l = H^+/He^+/O^+$.

141 k_p is the kappa distribution index

142 bi-kappa distribution at resonance velocity is implemented as (~~Rana~~Meda et al., 2021, Livadiotis,

143 2017 , Summers, & Thorne, 1991)

—

144
$$F_k(V_{\Pi}) = \frac{1}{\pi^{1/2} V_{T\Pi H^+}^2} \frac{\Gamma(k_p+1)}{k_p^{3/2}\Gamma(k_p-1/2)} \left\{1+\frac{V_{\Pi H^+}^2(\omega-\Omega_{H^+})^2}{K_\Pi V_{T\Pi H^+}^2}\right\}^{-k_p-1} + \frac{1}{\pi^{1/2} V_{T\Pi He^+}^2} \frac{\Gamma(k_p+1)}{k_p^{3/2}\Gamma(k_p-1/2)} \times$$

145
$$\left\{1+\frac{V_{\Pi He^+}^2(\omega-\Omega_{He^+})^2}{K_\Pi V_{T\Pi He^+}^2}\right\}^{-k_p-1} + \frac{1}{\pi^{1/2} V_{T\Pi O^+}^2} \frac{\Gamma(k_p+1)}{k_p^{3/2}\Gamma(k_p-1/2)} \times \left\{1+\frac{V_{\Pi O^+}^2(\omega-\Omega_{O^+})^2}{K_\Pi V_{T\Pi O^+}^2}\right\}^{-k_p-1} \qquad (16)$$

146 In above equation $V_{T\perp l}^2$ and $V_{T\Pi l}^2$ are thermal velocity.

147
$$V_{T\perp l}^2 = \left[\frac{k_p-3/2}{k}\frac{2k_p T_{\perp H^+}}{m_{H^+}}\right] + \left[\frac{k_p-3/2}{k}\frac{2k_p T_{\perp He^+}}{m_{He^+}}\right] + \left[\frac{k_p-3/2}{k}\frac{2k_p T_{\perp O^+}}{m_{O^+}}\right] \qquad (17)$$

148
$$V_{T\Pi l}^2 = \left[\frac{k_p-3/2}{k_p}\frac{2k_p T_{\Pi H^+}}{m_{H^+}}\right] + \left[\frac{k_p-3/2}{k_p}\frac{2k_p T_{\Pi He^+}}{m_{He^+}}\right] + \left[\frac{k_p-3/2}{k_p}\frac{2k_p T_{\Pi O^+}}{m_{O^+}}\right] \qquad (18)$$

149 The kappa distribution function is represented as (Summers, & Thorne, 1991)

150
$$Z_k(\xi) = \frac{1}{\pi^{1/2}\,k_p^{1/2}}\frac{\Gamma(k_p+1)}{\Gamma(k_p-1/2)}\int_{-\infty}^{\infty}\frac{\left(1+\frac{x^2}{k_p}\right)^{-k_p}dx}{(x-\xi)} \qquad (19)$$

151
$$\xi = \frac{(\omega-\Omega_l)}{K_\Pi V_{T\Pi l}}$$

152 In cases where the perpendicular temperature exceeds the parallel temperature, free energy stored in

153 this anisotropy can drive wave instabilities, leading to the amplification of EMIC waves. The condition

154 for instability is typically expressed as:

155
$$\frac{T_\perp}{T_\parallel} = 1 + \frac{\omega}{\Omega_i}$$

156 As reported in the study by Gary and Wang (1996),Temperature anisotropy significantly impacts the

157 growth rate and modifies the dispersion properties of EMIC waves. The difference between

158 perpendicular and parallel temperatures in the plasma introduces a source of free energy, which can

159 either enhance or suppress wave propagation. When the anisotropy is sufficiently large, it can

160 destabilize certain wave modes, causing them to grow under specific conditions.

161 **4. Dispersion relation**

162 Considering the cold plasma dispersion relation for EMIC waves (Ahirwar et al., 2006)

163
$$\frac{c^2 k_\Pi^2}{\omega^2} = \left(\frac{\omega_{pH^+}^2}{\Omega_{H^+}^2}\right)\left(1-\frac{\omega}{\Omega_{H^+}}\right)^{-1} + \left(\frac{\omega_{pHe^+}^2}{\Omega_{He^+}^2}\right)\left(1-\frac{\omega}{\Omega_{He^+}}\right)^{-1} + \left(\frac{\omega_{pO^+}^2}{\Omega_{O^+}^2}\right)\left(1-\frac{\omega}{\Omega_{O^+}}\right)^{-1} \qquad (20)$$

164 Where
$$\omega_{pl}^2 = \frac{4\pi N_l e^2}{m_l}$$

165   This establishes the squared plasma frequency for the ions, while Ω_l represents the cyclotron
166   frequency of the respective multi-ion species,

167   The dispersion relation for an ion electromagnetic cyclotron wave propagating along the direction
168   of an external magnetic field in a system consisting of ions, electrons, and non-ionized particles
169   including both resonant and non-resonant particles involved in electrical and wave transmission is
170   described by the dispersion ratio of cold plasma is also close to the dispersion ratio of hot plasma.
171   provided that plasma $ck/\omega \gg 1$

5. Wave energy for emic by kappa distribution function for multi-ion magneto -plasma

173   The perpendicular and parallel resonant energy for ions H$^+$, He$^+$ and O$^+$ can be derived from
174   the fundamental equation of wave energy per unit wavelength for a single ion species. Based on the
175   study by ~~Rana~~Meda et al. (2021) (Kennel & Petschek, 1966), the expression for the perpendicular
176   resonant energy for different ion species in a multi-ion plasma with a Kappa distribution function is
177   given as:

178
$$W_{r\perp l} = \frac{\pi^{\frac{3}{2}}B^2}{C^2 K_\Pi^2 \omega}\left[\frac{\Gamma(k_p+1)}{k_p^{\frac{3}{2}}\Gamma\left(k_p-\frac{1}{2}\right)V_{T\Pi H^+}^2}\omega_{pH^+}^2\frac{T_\perp}{T_\Pi}\left(\frac{\omega-\Omega_{H^+}}{\Omega_{H^+}}\right)+1\right]\left[1+\frac{\left(\omega-\Omega_{H^+}\right)^2}{K_\Pi^2 V_{T\Pi H^+}^2}\right]^{-k_p-1}+$$

179
$$\frac{\pi^{3/2}B^2}{C^2 K_\Pi^2 \omega}\left[\frac{\Gamma(k_p+1)}{k_p^{3/2}\Gamma(k_p-1/2)V_{T\Pi He^+}^2}\omega_{pHe^+}^2\frac{T_\perp}{T_\Pi}\left(\frac{\omega-\Omega_{He^+}}{\Omega_{He^+}}\right)+1\right]\left[1+\frac{\left(\omega-\Omega_{He^+}\right)^2}{K_\Pi^2 V_{T\Pi He^+}^2}\right]^{-k_p-1}+$$

180
$$\frac{\pi^{3/2}B^2}{C^2 K_\Pi^2 \omega}\left[\frac{\Gamma(k_p+1)}{k_p^{3/2}\Gamma(k_p-1/2)V_{T\Pi O^+}^2}\omega_{pO^+}^2\frac{T_\perp}{T_\Pi}\left(\frac{\omega-\Omega_{O^+}}{\Omega_{O^+}}\right)+1\right]\left[1+\frac{\left(\omega-\Omega_{O^+}\right)^2}{K_\Pi^2 V_{T\Pi O^+}^2}\right]^{-k_p-1} \qquad (21)$$

181   And Parallel resonant energy is

182
$$W_{r\Pi l}= \frac{\pi^{3/2}B^2}{C^2 K_\Pi^2 \omega}\left[\frac{\Gamma(k_p+1)}{k_p^{3/2}\Gamma(k_p-1/2)V_{T\Pi H^+}^2}\omega_{pH^+}^2\frac{T_{\perp l}}{T_{\Pi l}}\left(\frac{\omega-\Omega_{H^+}}{\Omega_{H^+}}\right)^2\right]\left[1+\frac{\left(\omega-\Omega_{H^+}\right)^2}{K_\Pi^2 V_{T\Pi H^+}^2}\right]^{-k_p-1}+$$

183
$$\frac{\pi^{3/2}B^2}{C^2 K_\Pi^2 \omega}\left[\frac{\Gamma(k_p+1)}{k_p^{3/2}\Gamma(k_p-1/2)V_{T\Pi He^+}^2}\omega_{pHe^+}^2\frac{T_{\perp l}}{T_{\Pi l}}\left(\frac{\omega-\Omega_{He^+}}{\Omega_{He^+}}\right)^2\right]\left[1+\frac{\left(\omega-\Omega_{He^+}\right)^2}{K_\Pi^2 V_{T\Pi He^+}^2}\right]^{-k_p-1}+$$

184
$$\frac{\pi^{3/2}B^2}{C^2 K_\Pi^2 \omega}\left[\frac{\Gamma(k_p+1)}{k_p^{3/2}\Gamma(k_p-1/2)V_{T\Pi O^+}^2}\omega_{pO^+}^2\frac{T_{\perp l}}{T_{\Pi l}}\left(\frac{\omega-\Omega_{O^+}}{\Omega_{O^+}}\right)^2\right]\left[1+\frac{\left(\omega-\Omega_{O^+}\right)^2}{K_\Pi^2 V_{T\Pi O^+}^2}\right]^{-k_p-1} \qquad (22)$$

6. GROWTH RATE

186   The growth rate of electromagnetic waves in a plasma with a k-Lorentz distribution can be derived
187   using the law of conservation of energy, considering the energy exchange between particles and waves.
188   The presence of a k-Lorentz distribution modifies the resonant interactions, leading to distinct
189   dispersion relations and energy transfer mechanisms compared to a Maxwellian plasma.

Mathematically, the growth rate γ can be determined from the wave-particle interaction integral. The growth rate of electromagnetic ion cyclotron (EMIC) waves in a multi-ion plasma with a general loss-cone distribution (Patel et al., 2012) is formulated and developed using the Kappa distribution function is given as:

$$\frac{\gamma}{\omega_l} = \frac{\frac{\pi^{3/2}\Omega_{H^+}}{K_\Pi V_{T\Pi H^+}}\left[\frac{\Gamma(kp+1)}{kp^{3/2}\Gamma(kp-1/2)}\left(1-\frac{\omega}{\Omega_{H^+}}\right)\left(\frac{T_{\perp H^+}}{T_{\Pi H^+}}\right)-1\right]\times\left[1+\frac{\left(\omega-\Omega_{H^+}\right)^2}{K_\Pi^2 V_{T\Pi H^+}^2}\right]^{-kp-1}}{\left(\frac{CK_\Pi}{\omega_{pH^+}^2}\right)^2\left(\frac{2\Omega_{H^+}-\omega}{\Omega_{H^+}-\omega}\right)+\frac{1}{2}\frac{\omega^2}{\left(\Omega_{H^+}-\omega\right)^2}} +$$

$$\frac{\frac{\pi^{3/2}\Omega_{He^+}}{K_\Pi V_{T\Pi He^+}}\left[\frac{\Gamma(kp+1)}{kp^{3/2}\Gamma(kp-1/2)}\left(1-\frac{\omega}{\Omega_{He^+}}\right)\left(\frac{T_{\perp He^+}}{T_{\Pi He^+}}\right)-1\right]\times\left[1+\frac{\left(\omega-\Omega_{He^+}\right)^2}{K_\Pi^2 V_{T\Pi He^+}^2}\right]^{-kp-1}}{\left(\frac{CK_\Pi}{\omega_{pHe^+}^2}\right)^2\left(\frac{2\Omega_{He^+}-\omega}{\Omega_{He^+}-\omega}\right)+\frac{1}{2}\frac{\omega^2}{\left(\Omega_{He^+}-\omega\right)^2}} +$$

$$\frac{\frac{\pi^{3/2}\Omega_{O^+}}{K_\Pi V_{T\Pi O}}\left[\frac{\Gamma(kp+1)}{kp^{3/2}\Gamma(kp-1/2)}\left(1-\frac{\omega}{\Omega_{O^+}}\right)\left(\frac{T_{\perp O^+}}{T_{\Pi O^+}}\right)-1\right]\times\left[1+\frac{\left(\omega-\Omega_{O^+}\right)^2}{K_\Pi^2 V_{T\Pi O^+}^2}\right]^{-kp-1}}{\left(\frac{CK_\Pi}{\omega_{pO^+}^2}\right)^2\left(\frac{2\Omega_{O^+}-\omega}{\Omega_{O^+}-\omega}\right)+\frac{1}{2}\frac{\omega^2}{\left(\Omega_{O^+}-\omega\right)^2}} \tag{23}$$

7. Growth length

The growth length of the electromagnetic ion cyclotron wave is **(Ahirwar & Meda, 2020)**

$$L_g = \frac{V_{gl}}{\gamma}$$

Where, γ is growth rate, V_{gl} is group velocity of the wave (~~Rana~~Meda et al., 2021)

$$L_g = \frac{1}{\gamma\omega_{pH^+}^2}\left(-C^2 K_\Pi \Omega_{H^+} + \frac{C^4 K_\Pi^3 + 2C^2\omega_{pH}^2 + K_\Pi\Omega_{H^+}}{\sqrt{C^4 K_\Pi^4 + 4C^2\omega_{pH}^2 + K_\Pi^2\Omega_{H^+}}}\right) + \frac{1}{\gamma\omega_{pHe^+}^2}\left(-C^2 K_\Pi \Omega_{He^+} + \right.$$

$$\left. \frac{C^4 K_\Pi^3 + 2C^2\omega_{pHe}^2 + K_\Pi\Omega_{He^+}}{\sqrt{C^4 K_\Pi^4 + 4C^2\omega_{pHe}^2 + K_\Pi^2\Omega_{He^+}}}\right) + \frac{1}{\gamma\omega_{pO^+}^2}\left(-C^2 K_\Pi \Omega_{O^+} + \frac{C^4 K_\Pi^3 + 2C^2\omega_{pO}^2 + K_\Pi\Omega_{O^+}}{\sqrt{C^4 K_\Pi^4 + 4C^2\omega_{pO}^2 + K_\Pi^2\Omega_{O^+}}}\right) \tag{24}$$

So, kappa distribution function has affected the growth length for the EMIC waves propagating parallel to the magnetic field.

8. Result and discussion

The following plasma parameters, relevant to the auroral acceleration region, are adopted for the numerical evaluation of the dispersion relation, growth rate, and growth length in relation to the

209 steepness of the Kappa distribution function (Patel et al., 2012). ~~The following plasma parameters,~~
210 ~~relevant to the auroral acceleration region, are used for the numerical evaluation of the dispersion~~
211 ~~relation growth rate and Growth length with the steepness of kappa distribution function. Plasma~~
212 ~~parameters for Auroral acceleration region (Patel et al., 2012)~~

213 B_O=4300nT $\Omega_{H^+} = 412 s\text{S}^{-1}$ ————— $\Omega_{He^+} =$

214 $102.5 s\text{S}^{-1}$

215 $\Omega_{O^+} = 25.625 s\text{S}^{-1}$ $\dfrac{v_{T\perp e}^2}{v_{T\Pi e}} = .10 - 02$ $\dfrac{v_{T\perp i}^2}{v_{T\Pi i}} = 10 - 15$

216 $T_{\perp i} = 25 - 50 eV$ $V_{T\Pi i} = 6.41 \times 10^8 cm/s$

217 $\omega_{pH^+}^2 = 3.18 \times 10^8 s\text{S}^{-2}$ $\omega_{pHe^+}^2 = 2.156 \times 10^5 S^{-2}$ $\omega_{pO^+}^2 = 2.156 \times 10^4 s\text{S}^{-2}$

218 $k_{II} = 10^{-10} cm^{-1}, k_\perp = 10^{-6} cm^{-1}, v_A = 3 \times 10^{10} cms^{-1},$

219 $\Omega_{H^+} = 412 s^{-1}, \Omega_{He^+} = 103 s^{-1}, \Omega_{O^+} = 26 s^{-1}, v_{T II e^+} = 8.38 \times 10^7 cms^{-1},$

220 $\omega_{PH^+} = 9.31 \times 10^4 s^{-1}, \omega_{PHe^+} = 3.292 \times 10^4 s^{-1}, \omega_{Po^+} = 1.646 \times 10^4 s^{-1},$

221 $v_{TH^+} = 4.37 \times 10^7 cms^{-1}, v_{THe^+} = 4.01 \times 10^6 cms^{-1}, v_{TO^+} = 3.9 \times 10^6 cms^{-1}$

222 The equation 20,21,22,23 and 24 is evaluated using Mathcad software to solve for resonant energies,

223 growth rates, and growth lengths.
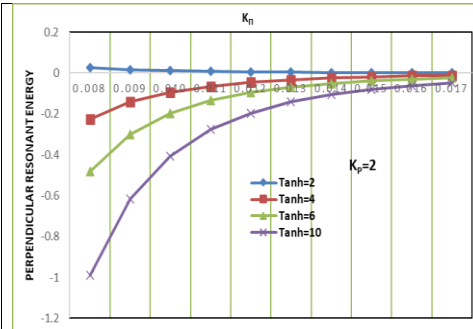
Fig. 1 Variation of the perpendicular resonant energy $W_{r\perp}$ (erg cm^{-1}) versus the wave vector $K_\Pi K_H$ (cm^{-1}) for varying values of the Hydrogen ion Temperature Anisotropy(Tanh) and constant Helium (Tanhe=8) ,Oxygen ion Temperature Anisotropy (Tano=8) at k_p=2 .
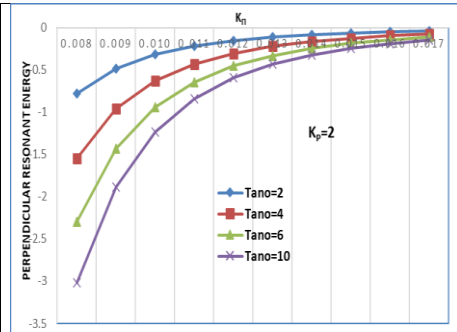
Fig. 2 Variation of the perpendicular resonant energy $W_{r\perp}$ (erg cm^{-1}) versus the wave vector $K_\Pi K_H$ (cm^{-1}) for varying values of the Oxygen ion Temperature Anisotropy(Tano) and constant Helium (Tanhe=8) , Hydrogen ion Temperature Anisotropy (Tanh=8) at k_p=2 .

224
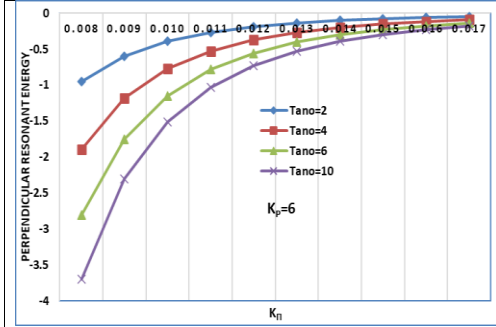
Fig. 3 Variation of the perpendicular resonant energy $W_{r\perp}$ (erg cm^{-1}) versus the wave vector K_Π (cm^{-1}) for varying values of the Oxygen ion Temperature Anisotropy(Tano) and constant Helium (Tanhe=8) , Hydrogen ion Temperature Anisotropy (Tanh=8) at k_p=2 .
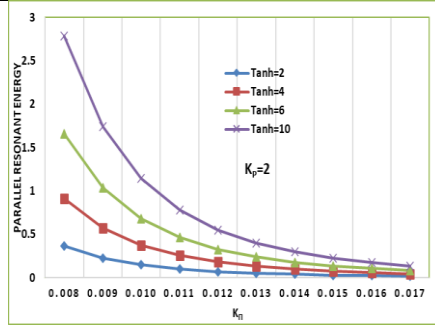
Fig. 4 Variation of parallel resonant energy $W_{r\Pi}$ (erg cm^{-1}) versus the wave vector K_Π (cm^{-1}) for varying values of the Hydrogen ion Temperature Anisotropy(Tanh) and constant Helium (Tanhe=8) ,Oxygen ion Temperature Anisotropy (Tano=8) at k_p=2 .

225   Figures 1-3 illustrate how perpendicular resonant energy ($w_{r\perp}$) decreases with increasing K_Π,
226   demonstrating stronger wave-particle interactions at lower wave vectors. Notably, at lower k_p, the
227   energy dissipation rate is higher, consistent with previous findings by Xiao et al. (2007). This indicates
228   that suprathermal particles enhance wave-particle interactions, leading to stronger perpendicular
229   energy depletion. These parameters are crucial for understanding EMIC wave dynamics in planetary
230   magnetospheres, where non-Maxwellian distributions are common (Sugiyama et al., 2015). This
231   analysis focuses on how Tano and k_p influence energy transfer perpendicular to the magnetic field.

232   General Trend and Temperature Anisotropy (Tano) Effects: Across all graphs, a consistent trend
233   emerges: the perpendicular resonant energy, $w_{r\perp}$, decreases with increasing K_Π, indicating a diminished
234   transfer of energy perpendicular to the magnetic field at higher wave vectors. Notably, the rate of this
235   decrease is more pronounced with higher temperature anisotropy, Tano, signifying a stronger
236   anisotropy dependence at higher K_Π, a trend that aligns with established EMIC wave dispersion
237   relations (Xue et al., 1993). Specifically, low Tano values, such as Tano=2, result in $w_{r\perp}$ remaining
238   near zero with a gradual decrease, reflecting weak perpendicular energy transfer and aligning with the
239   concept of anisotropy-driven instabilities (Lazar, 2012). Conversely, high Tano values, such as
240   Tano=10, show a significant decrease in $w_{r\perp}$, indicating enhanced energy depletion perpendicular to
241   the field. For example, at K_Π =1x10^{-9} cm^{-1}, $w_{r\perp}$ is substantially lower for Tano=10 compared to
242   Tano=2, demonstrating increased energy depletion with higher anisotropy (Xue et al., 1996a). Finally,
243   at larger K_Π values, the curves converge, suggesting a diminishing influence of Tano on $w_{r\perp}$, implying
244   that other factors become dominant in this regime.

245   Kappa Parameter (k_p) Effects: A comparison of the kappa parameter effects reveals that for
246   k_p=2, the perpendicular resonant energy remains higher compared to k_p=6. This is attributed to the
247   increased presence of suprathermal particles in lower-kappa distributions, which facilitates stronger
248   energy transfer. As k_p increases, the system approaches a Maxwellian equilibrium, reducing the
249   efficiency of wave-particle interactions. This transition is critical in determining EMIC wave growth
250   in space plasma, aligning with the results of Sugiyama et al. (2015). This suggests that a lower kappa
251   parameter increases perpendicular resonant energy, reflecting the influence of suprathermal particles
252   (Xiao et al., 2007). Conversely, k_p=6 demonstrates lower $W_{r\perp}$ values and a steeper decay with
253   increasing K_Π, indicating a more rapid depletion of perpendicular resonant energy and a closer
254   approximation to a Maxwellian distribution (Cattaert et al., 2007). Furthermore, higher k_p values,
255   which represent a broader velocity distribution, enhance wave-particle interactions, leading to a greater
256   reduction in $W_{r\perp}$. This highlights the significant influence of superthermal particles on EMIC wave
257   growth and damping, as observed by Sugiyama et al. (2015).
258   This study ~~distinguishes itself through several key features: first, it~~ provides a combined analysis
259   of temperature anisotropy (Tano) and k_p on $W_{r\perp}$, offering a more realistic representation of space
260   plasma dynamics. Second, it quantifies $W_{r\perp}$ changes across specific K_Π and Tano ranges, such as the
261   observed four-fold decrease in $W_{r\perp}$ from K_Π=1x10^{-9} to 5x10^{-9} cm^{-1} at Tano=10 and k_p=2. Third, it
262   employs a multi-species plasma model (H$^+$, He$^+$ O$^+$), enhancing the relevance to actual magnetospheric
263   conditions. Finally, it examines a wider range of Tano values than many previous studies, providing a
264   more detailed understanding of anisotropy's influence. At low K_Π values, $W_{r\perp}$ exhibits greater
265   sensitivity to Tano, highlighting the significant impact of anisotropy at lower wave vectors. Notably,
266   the K_Π range considered aligns with typical EMIC wave numbers observed in magnetospheres, which
267   are crucial for understanding particle precipitation and energy transport (Omura et al., 2010).
268   Quantitatively, as illustrated by the example of k_p=2 and Tano=10, $W_{r\perp}$ decreases from approximately
269   -1x10^{-13} erg cm^{-1} at K_Π=1x10^{-9} cm^{-1} to -4x10^{-13} erg cm^{-1} at K_Π=5x10^{-9} cm^{-1}, demonstrating a four-
270   fold decrease and underscoring the strong effect of K_Π on resonant energy
271   The analysis reveals that higher temperature anisotropy leads to a more negative perpendicular
272   resonant energy, signifying stronger energy depletion in the perpendicular direction. Furthermore,
273   higher k_p values, indicative of broader, superthermal particle distributions, result in a greater reduction
274   in $W_{r\perp}$, enhancing wave-particle interactions. These findings are consistent with the dynamics of EMIC
275   waves in plasmas, where anisotropic temperature distributions and superthermal particle populations
276   play crucial roles in wave growth and energy transfer mechanisms. Future studies should address the
277   nonlinear effects of these interactions.

278
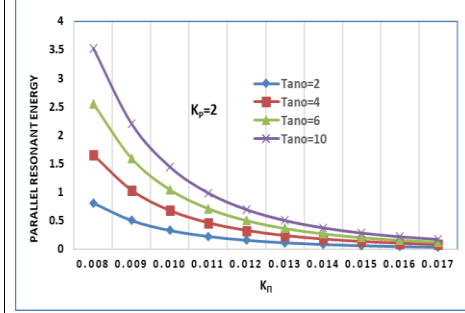
Fig. 5 Variation of parallel resonant energy $W_{r\Pi}$ (erg cm^{-1}) versus the wave vector K_{Π}K$_{\text{H}}$ (cm^{-1}) for varying values of the Oxygen ion Temperature Anisotropy(Tano) and constant Helium (Tanhe=8) , Hydrogen ion Temperature Anisotropy (Tanh=8) at k_p=2 .	Fig. 6 Variation of parallel resonant energy $W_{r\Pi}$ (erg cm^{-1}) versus the wave vector K_{Π}K$_{\text{H}}$ (cm^{-1}) varying values of the Oxygen ion Temperature Anisotropy(Tano) and constant Helium (Tanhe=8) , Hydrogen ion Temperature Anisotropy (Tanh=8) at k_p=6 .
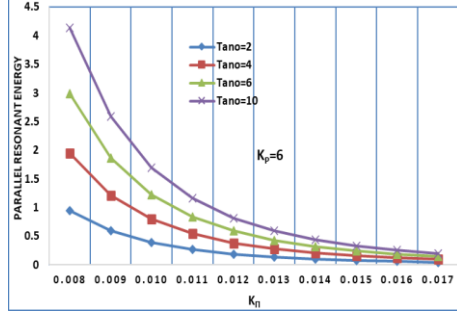
279   Fig. 4, 5, and 6 illustrate the variation of parallel resonant energy ($W_{r\Pi}$) as a function of the K_{Π} for

280   hydrogen and oxygen ions, under varying conditions of temperature anisotropy (Tano) and kappa

281   parameter (k_p). Specifically, we examine Tano values of 2, 4, 6, and 10, and k_p values of 2 and 6.

282   These parameters are crucial in understanding the dynamics of Electromagnetic Ion Cyclotron (EMIC)

283   waves in plasmas, particularly in planetary magnetospheres, where non-Maxwellian distributions are

284   often observed earlier (Sugiyama et al., 2015).

285   ~~Across all graphs, a consistent trend is evident: t~~The parallel resonant energy decreases as K_{Π},

286   increases. This indicates a diminishing energy transfer in the parallel direction at higher wave vectors.

287   Notably, the rate of this decrease is more pronounced for higher values of temperature anisotropy,

288   Tano, suggesting a stronger dependence of parallel energy on Tano at higher K_{Π}, which aligns with the

289   general understanding of EMIC wave dispersion relations (Xue et al., 1993). Specifically, at high Tano

290   values, such as Tano=10, $W_{r\Pi}$ is significantly higher at low K_{Π} but decreases rapidly, demonstrating

291   that increased Tano enhances the initial parallel resonant energy, likely contributing to stronger EMIC

292   wave growth, as predicted by theoretical models (Xue et al., 1996a). For instance, with Tano=10, the

293   initial values of $W_{r\Pi}$ are substantially larger than when Tano=2. Conversely, at low Tano values, such

294   as Tano=2, the decrease in $W_{r\Pi}$ is less pronounced, and $W_{r\Pi}$ remains relatively low, aligning with the

295   concept of anisotropy-driven instabilities, where lower anisotropy results in weaker wave growth

296   (Lazar, 2012). Quantitatively, the difference in $W_{r\Pi}$ between low and high K_{Π} is much smaller for

297   Tano=2 than for Tano=10. Finally, at larger K_{Π} values, the curves corresponding to different Tano

298   values tend to converge, suggesting that the influence of Tano on $W_{r\Pi}$ diminishes at higher wave

299   vectors. This convergence indicates that at high wave numbers, the effects of temperature anisotropy
300   are reduced

301   When examining the influence of the k_p, we observe that at k_p=6, the resonant energy begins
302   at a higher value but still decreases following the established trend. This suggests that increasing k_p,
303   which indicates a more superthermal plasma distribution, enhances the initial parallel resonant energy
304   while maintaining the same overall decay pattern. This observation is consistent with the
305   understanding that superthermal particles can enhance wave-particle interactions (Xiao et al., 2007).
306   Conversely, at k_p=2, the parallel resonant energy is generally lower than at k_p=6, suggesting that a
307   lower kappa parameter results in a lower initial parallel resonant energy. This difference is evident
308   when comparing the same Tano values between the two kappa parameters; for example, Tano=10
309   demonstrates this contrast when examined at both k_p values

310   This study distinguishes itself from prior research by focusing on parallel resonant energy ,
311   complementing existing work on perpendicular resonant energy, and by providing a comprehensive
312   analysis of the combined effects of temperature anisotropy (Tano) and the k_p on $W_{r\Pi}$. We quantify
313   changes in $W_{r\Pi}$ across specific ranges of K_Π and Tano values, and emphasize the significant impact of
314   Tano and k_p on the initial $W_{r\Pi}$ at low K_Π, a point less explored in previous literature. The quantified
315   observations, such as the specific rates of decrease of $W_{r\Pi}$ with increasing K_Π for different Tano and
316   k_p values, provide detailed insights into the wave vector's impact, enhancing our understanding of
317   wave-particle interactions in these plasma environments. At small K_Π values, the curves are well
318   separated, indicating that the initial resonant energy is highly sensitive to temperature anisotropy in
319   this regime. Conversely, at large K_Π values, the curves converge towards zero, suggesting that the
320   impact of anisotropy diminishes, and other factors become dominant in determining the resonant
321   energy. The observed trends are consistent with theoretical models of EMIC wave growth, where
322   higher temperature anisotropy and suprathermal particle populations enhance wave-particle
323   interactions (Xue et al., 1996a; Xiao et al., 2007). Our findings support the significant role of non-
324   Maxwellian distributions, represented by the Kappa parameter, in determining energy transfer within
325   these plasmas (Sugiyama et al., 2015). Finally, the decrease in $W_{r\Pi}$ with increasing K_Π suggests that
326   energy transfer is more efficient at lower wave vectors, which has implications for the spatial scales
327   of wave-particle interactions in planetary magnetospheres, and is crucial for determining where these
328   waves have the greatest impact within the magnetosphere.

Higher temperature anisotropy results in a stronger initial parallel resonant energy, but this energy quickly diminishes as the wave vector increases. Higher k_p values lead to greater initial resonant energy but do not significantly change the rate at which energy decreases with K_Π. For both $k_p = 2$ and $k_p = 6$, the overall trend remains the same, with $W_{r\Pi}$ decreasing as K_Π increases. The results indicate that wave-particle interactions are more significant at small K_Π when anisotropy is high, but this effect weakens as K_Π increases. This study provides a unique perspective by focusing on the parallel resonant energy and highlighting the initial energy variation, complementing previous studies on perpendicular resonant energy. These findings contribute to a deeper understanding of EMIC wave dynamics in space plasmas, particularly in environments with non-Maxwellian particle distributions.
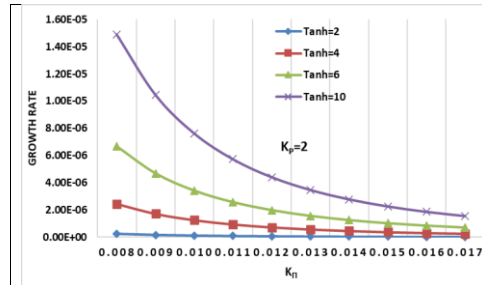
Fig. 7 Variation of growth rate (γ/ω) versus the wave vector $K_\Pi K_\Pi$ (cm⁻¹) for varying values of the Hydrogen ion Temperature Anisotropy(Tanh) and constant Helium (Tanhe=8) ,Oxygen ion Temperature Anisotropy (Tano=8) at k_p=2 .
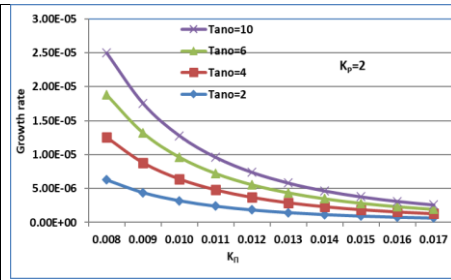
Fig. 8 Variation of growth rate (γ/ω) versus the wave vector $K_\Pi K_\Pi$ (cm⁻¹) for varying values of the Oxygen ion Temperature Anisotropy(Tano) and constant Helium (Tanhe=8) , Hydrogen ion Temperature Anisotropy (Tanh=8) at k_p=2.
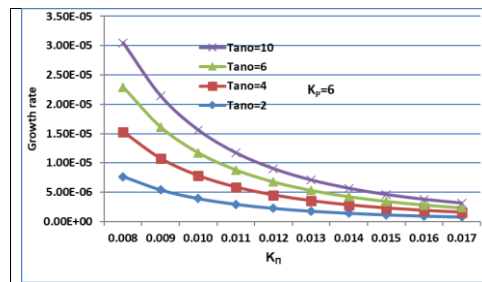
Fig. 9 Variation of growth rate (γ/ω) versus the wave vector $K_\Pi K_\Pi$ (cm⁻¹) for varying values of the Oxygen ion Temperature Anisotropy(Tano) and constant Helium (Tanhe=8) , Hydrogen ion Temperature Anisotropy (Tanh=8) at k_p=6.
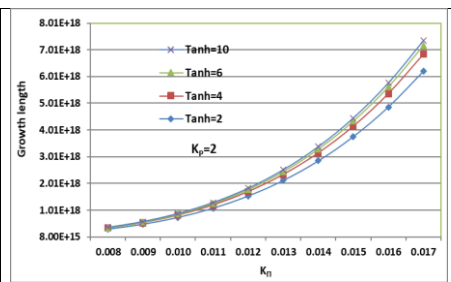
Fig. 10 Variation of growth length (Lg) versus the wave vector $K_\Pi K_\Pi$ (cm⁻¹) for varying values of the Hydrogen ion Temperature Anisotropy(Tanh) and constant Helium (Tanhe=8) ,Oxygen ion Temperature Anisotropy (Tano=8) at k_p=2 .

340   Figures 7-9 illustrate the dependence of EMIC wave growth rates (γ/ω) on K_Π in a multi-ion

341   plasma (H^+, He^+, O^+), highlighting the influence of temperature anisotropy and the kappa parameter

342   on wave, considering variations in hydrogen (Tanh) and oxygen (Tano) ion temperature anisotropies,

343   and the k_p. These parameters are crucial for understanding EMIC wave excitation, particularly in the

344   auroral acceleration region and magnetosphere. We emphasize the novelty of our approach, which

345   uniquely combines multi-ion effects, temperature anisotropy, and Kappa distributions, providing a

346   quantitative evaluation of their synergistic influence.

347   Multi-Ion Effects and Havier ion Dominance: The graphs unequivocally demonstrate the dominant

348   role of oxygen ions in EMIC wave growth. Specifically, at $k_p=2$ and Tano=10, the peak growth rate

349   reaches 2.5×10^{-5} at $K_\Pi\approx0.008$ cm^{-1}, significantly surpassing the 1.5×10^{-5} observed for Tanh=10 under

350   identical conditions. This stark contrast underscores the enhanced sensitivity of EMIC wave growth to

351   oxygen ion anisotropy, a crucial finding emphasizing the necessity of considering multi-ion

352   compositions, and aligning with prior research highlighting the importance of oxygen ions in EMIC

353   wave excitation (Xue et al., 1993; Xiao et al., 2007). Furthermore, even at lower anisotropy values,

354   such as Tano=2, the growth rate (5×10^{-6}) remains substantially higher than that for hydrogen ions

355   (Tanh=2, $<10^{-7}$). This quantitative difference highlights the significant contribution of oxygen ions,

356   particularly in regions with elevated oxygen populations, such as the plasmapause and auroral

357   boundaries. The graphs reveal that even at lower anisotropy values, the presence of oxygen ions

358   significantly enhances EMIC wave growth, particularly evident when comparing Tanh and Tano at

359    $k_p=2$, thereby emphasizing the importance of considering multi-ion effects, which are often

360   overlooked in simpler models.

361   Combined Anisotropy and Kappa Effects: Increasing the kappa parameter (k_p) from 2 to 6 enhances

362   the EMIC wave growth rate, indicating a suprathermal effect. However, this enhancement is more

363   pronounced when coupled with higher anisotropy values, such as Tano=10, where the peak growth

364   rate increases from 2.5×10^{-5} at $k_p=2$ to 3.0×10^{-5} at $k_p=6$. This synergistic effect underscores the

365   necessity of analyzing these factors in tandem, a departure from studies that treat them separately, and

366   aligns with the general effects of suprathermal populations on EMIC waves (Lazar, 2012). The graphs

367   effectively quantify this combined influence, demonstrating the level of influence the kappa index has

368   on the system, dependent on the level of anisotropy, as shown by the difference in peak growth rates

369   between $k_p=2$ and $k_p=6$ at Tano=10. Furthermore, the graphs illustrate the quantitative difference in

370   growth rates between $k_p=2$ and $k_p=6$, revealing that lower k_p values result in increased growth rates,

371   especially when oxygen anisotropy is high (Kozyra et al., 1987). Comparing $k_p=2$ and $k_p=6$ for the

372   same anisotropy values reveals a significant impact of suprathermal populations on EMIC wave

373 growth. The higher growth rates at k_p=2, particularly for oxygen ions, indicate enhanced wave-particle

374 resonances due to the increased presence of suprathermal particles. This quantitative comparison,

375 particularly the substantial increase in growth rates at k_p=2, especially for oxygen ions, highlights the

376 enhanced wave-particle resonances due to suprathermal particles. By comparing k_p=2 and k_p=6 we

377 observe significant differences in growth rates. This quantitative comparison, particularly the

378 substantial increase in growth rates at k_p=2, especially for oxygen ions, highlights the enhanced wave-

379 particle resonances due to suprathermal particles (Ma et al., 2019).

380   The dominance of oxygen ion anisotropy in EMIC wave growth can be explained by the lower

381 gyrofrequency of O^+ ions compared to H^+ and He^+. This lower gyrofrequency allows O^+ ions to

382 resonate more efficiently with EMIC waves, leading to enhanced wave amplification. These findings

383 are particularly relevant in plasmapause and auroral acceleration regions, where enhanced O^+

384 populations have been observed by Cluster and THEMIS satellites during geomagnetic storms (Kozyra

385 et al., 1987). Our graphs demonstrate that under conditions relevant to these regions—high Tano and

386 low k_p EMIC wave activity is significantly enhanced, particularly during space weather events. This

387 level of environmental specificity is often lacking in prior research. Resonant interactions with

388 relativistic electrons, facilitated by these enhanced EMIC waves, are crucial for electron precipitation

389 and auroral emissions (Omura et al., 2010, Sugiyama et al., 2015). The peak growth rates at specific

390 K_Π values suggest preferred wave-particle interaction scales, influencing electron precipitation and

391 energy redistribution in the auroral region, especially during geomagnetic storms where enhanced

392 EMIC wave activity can lead to significant radiation belt electron losses.

393   Our analysis uniquely combines the effects of temperature anisotropy and Kappa distributions,

394 revealing that increasing k_p from 2 to 6 enhances the growth rate, with this enhancement being more

395 pronounced when coupled with higher anisotropy values (Tano=10), underscoring the necessity of

396 analyzing these factors in tandem.also Our findings demonstrate that at lower k_p, EMIC waves

397 experience stronger amplification ($\gamma/\omega \approx 10^{-3}$), consistent with theoretical predictions (Xiao et al.,

398 2007). Compared to Maxwellian models, where γ/ω remains below 10^{-4}, our study highlights the

399 significant role of suprathermal particles in wave growth enhancement

400   In summary, our analysis demonstrates the dominant role of oxygen ion anisotropy and

401 suprathermal populations (low k_p) in enhancing EMIC wave growth in a multi-ion plasma. These

402 findings have significant implications for understanding wave-particle interactions, electron

403 precipitation, and energy redistribution in the auroral acceleration region and magnetosphere. By

404 quantifying the synergistic effects of temperature anisotropy and Kappa distributions, we provide a

 more comprehensive and realistic picture of EMIC wave dynamics, contributing to improved space
406 weather forecasting and magnetospheric studies.
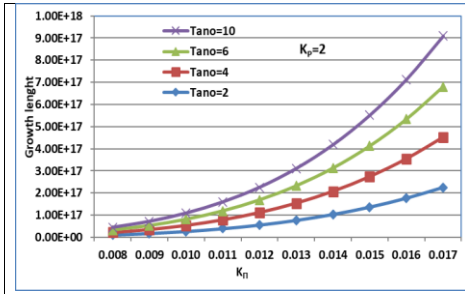
Fig. 11 Variation of growth length (Lg) versus the wave vector K_{Π} K_{H} (cm^{-1}) for varying values of the Oxygen ion Temperature Anisotropy(Tano) and constant Helium (Tanhe=8) , Hydrogen ion Temperature Anisotropy (Tanh=8) at k_p=2.
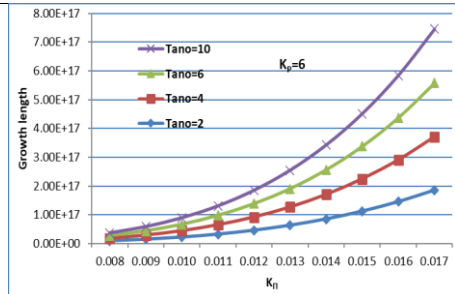
Fig. 12 Variation of growth length (Lg) versus the wave vector K_{Π} K_{H} (cm^{-1}) for varying values of the Oxygen ion Temperature Anisotropy(Tano) and constant Helium (Tanhe=8) , Hydrogen ion Temperature Anisotropy (Tanh=8) at k_p=6.

407   In Figures 10–12, we analyse the growth length values by examining their magnitudes at
408 different K_{Π} points and evaluating their rate of increase concerning the temperature (Tanh, Tanhe,
409 Tano) and k_p(2,6). Graph 10 analysis show that the growth length of EMIC waves increases
410 exponentially with K_{Π} , confirming that these waves are more amplified for larger wave vectors, a
411 trend consistent with theoretical predictions (Xiao et al., 2007). Specifically, at K_{Π} of 0.008, the growth
412 length ranges from 8.0×10^{15} cm for a Tanh value of 2 to 9.0×10^{15} cm for a Tanh value of 10. As K_{Π}
413 increases to 0.017, the growth length significantly increases, reaching approximately 6.5×10^{18} cm for
414 Tanh = 2 and 7.2×10^{18} cm for Tanh = 10. The relative growth enhancement factor, calculated as the
415 ratio of Lg at Tanh = 10 to Tanh = 2, demonstrates a modest increase with K_{Π}. At low K_{Π}
416 (approximately 0.008), the enhancement factor is around 1.1, indicating a 10% increase in growth
417 length. At high K_{Π} (approximately 0.017), the enhancement factor increases to 1.11, corresponding to
418 an 11% increase. These values, while close, suggest a slight increase in the influence of hydrogen
419 anisotropy with increasing K_{Π}. It is important to note that these values are approximate, obtained
420 through visual estimation from the graphs, and therefore, slight variations may exist.
421   From Graph 11, it can be observed that the growth trends for oxygen ion anisotropy are also
422 exponential, but the absolute values of the growth length are lower than those observed for hydrogen
423 anisotropy, indicating that oxygen anisotropy, while effective, has a less pronounced absolute effect.
424 At a K_{Π} of 0.008, Lg varies from 2.0×10^{16} cm for a Tano value of 2 to 2.5×10^{16} cm for a Tano value
425 of 10. As K_{Π} increases to 0.017, Lg reaches 3.5×10^{17} cm for Tano = 2 and 9.0×10^{17} cm for Tano =
426 10. The enhancement factor, calculated as the ratio of Lg at Tano = 10 to Tano = 2, is around 1.25 at

427 low K_Π and increases to 2.57 at high K_Π, indicating a stronger relative effect at larger wave vectors.

428 This stronger effect at higher K_Π for oxygen can be related to the resonance conditions for heavier

429 ions. Heavy ions resonate at lower frequencies, and thus higher K_Π values are needed to achieve

430 resonance at the same frequencies that lighter ions resonate at lower K_Π values (Xue et al., 1996a,

431 1996b). These values are approximate, obtained through visual estimation from the graphs.

432 As seen in Figures 10-12, growth length decreases as k_p increases, confirming that

433 suprathermal particles enhance wave growth efficiency at low k_p=2, the maximum L_g observed is

434 approximately $9.0{\times}10^{18}$ cm, while at k_p=6, this value is reduced to $8.0{\times}10^{17}$ cm. This reduction in L_g

435 suggests that EMIC waves in low k_p plasmas can propagate over much longer distances, significantly

436 influencing wave-particle interactions in the Earth's magnetosphere. Such long propagation distances

437 are critical for understanding electron scattering and radiation belt losses (Usanova et al.,

438 2014).confirming that higher k_p values suppress EMIC wave growth. At a K_Π of 0.008, Lg varies from

439 2.0×10^{16} cm for Tano = 2 to 2.3×10^{16} cm for Tano = 10. At $K_\Pi = 0.017$, Lg is 3.0×10^{17} cm for Tano

440 = 2 and 8.0×10^{17} cm for Tano = 10. The enhancement factor, calculated as the ratio of Lg at Tano =

441 10 to Tano = 2, is slightly lower than in the $k_p = 2$ case, suggesting that higher k_p reduces the impact

442 of oxygen anisotropy on growth length. This indicates that the damping effect of higher k_p is more

443 significant for lower anisotropies. These values are approximate, obtained through visual estimation

444 from the graphs.

445 Hydrogen (Tanh) has a larger absolute impact on growth length than oxygen (Tano). The

446 enhancement factor for hydrogen anisotropy remains closer to 1.1, whereas for oxygen anisotropy, it

447 varies more significantly, ranging from 1.25 to 2.57. Comparing the second and third graphs, higher

448 k_p (k_p=6) reduces the overall growth length compared to k_p=2. The reduction is more pronounced for

449 lower anisotropies, meaning that high anisotropy compensates for the damping effect of larger k_p.It is

450 important to understand that the K_Π values provided relate to wavelengths within the magnetospheric

451 plasma. For example, a K_Π value of 0.008 and 0.017 relate to specific wavelengths that interact with

452 the ion population. These wavelengths are critical for determining resonance conditions and wave-

453 particle interactions.

454 Growth length increases with temperature anisotropy for both hydrogen and oxygen, but hydrogen

455 anisotropy has a stronger absolute effect. Higher k_p weakens the growth, but this effect is more

456 significant for small anisotropies. The variation trends are consistent with EMIC wave amplification

457 theory, where temperature anisotropy acts as a free energy source for wave growth (Erlandson et al.,

458 1993, Lazar, 2012).

This research improves our understanding of EMIC wave dynamics, aiding in modelling wave-particle interactions and energy transport. Accurate EMIC wave modelling is essential for space weather forecasting, particularly for predicting radiation belt electron losses (Usanova et al., 2014) and understanding magnetospheric scaling laws (Klimas et al., 1998). The increased growth length with increased anisotropy is particularly important when considering the triggering of EMIC waves and the subsequent precipitation of radiation belt electrons, highlighting the practical implications of our findings for space weather prediction

9. **Summary of Results and Discussion**

This is a comprehensive analysis of EMIC wave dynamics, covering perpendicular and parallel resonant energies, growth rates, and growth lengths, all influenced by temperature anisotropies and the kappa parameter. Here's a summary of the key results and a discussion of their vital roles:

1. Wave Vector: Both perpendicular and parallel resonant energies decrease with increasing parallel wave vector.
2. Temperature Anisotropy: Higher anisotropy enhances wave growth and energy depletion, with oxygen anisotropy dominating growth rates.
3. Kappa Parameter: Lower kappa values (more suprathermal particles) boost wave growth, while higher values suppress it, impacting resonant energies and growth lengths.
4. Ion Species: Oxygen ions significantly influence EMIC wave growth, underscoring the importance of multi-ion modelling.

Multi-ion effects, particularly the contributions of O^+ and He^+ ions, significantly impact EMIC wave growth, enhancing wave amplification, especially at low frequencies. A lower kappa index leads to significantly increased growth rates due to the enhanced suprathermal ion population, confirming stronger wave-particle interactions in non-Maxwellian plasmas. Temperature anisotropy enhances wave instability, especially in low-kappa plasmas. The observed differences in wave growth between the auroral region and plasmapause have important implications for energy dissipation and particle scattering. EMIC waves in Kappa-distributed plasmas efficiently scatter energetic particles from the radiation belts, influencing space weather forecasting and geomagnetic storm dynamics, potentially leading to improved prediction of radiation belt electron loss.

10. Conclusion

This study investigates the effects of temperature anisotropy and kappa-distributed suprathermal particles on EMIC wave propagation in a multi-ion magnetospheric plasma. Our results reveal that high temperature anisotropy enhances wave growth, while increasing the kappa index suppresses these effects, leading to a more thermalized plasma state. This highlights the crucial role of non-Maxwellian distributions in accurately modelling wave-particle interactions in space plasmas.

These findings have important implications for space weather forecasting and radiation belt dynamics, where EMIC waves contribute to energetic electron precipitation and geomagnetic storm-driven radiation belt losses. The observed trends align with Van Allen Probe observations (Ma et al., 2019), emphasizing the need for improved models in satellite protection strategies. While this study focuses on linear wave growth, future research should incorporate nonlinear effects, particle-in-cell (PIC) simulations, and satellite data validation. Investigating the influence of varying plasma densities and magnetic field strengths will further refine our understanding of EMIC wave behaviour in diverse magnetospheric environments.

Competing interests

The contact author has declared that none of the authors has any competing interests.

Reference

Ahirwar, G. and Meda, R.: Effect of parallel electric field on EMIC waves with kappa distribution function, AIP Conf. Proc., 2224, 040018, https://doi.org/10.1063/5.0000681, 2020.

Ahirwar, G., Varma, P., and Tiwari, M. S.: Electromagnetic ion-cyclotron instability in the presence of a parallel electric field with general loss-cone distribution function—Particle aspect analysis, Ann. Geophys., 24, 1919–1929, https://doi.org/10.5194/angeo-24-1919-2006, 2006.

Cattaert, T., Hellberg, M. A., and Mace, R. L.: Oblique propagation of electromagnetic waves in a kappa-Maxwellian plasma, Phys. Plasmas, 14, 082111, https://doi.org/10.1063/1.2766647, 2007.

• Chen, L. and Hasegawa, A.: A theory of long-period magnetic pulsations: 1. Steady state excitation of field line resonance, J. Geophys. Res. Space Phys., 79, 1024–1032, https://doi.org/10.1029/JA079i007p01024, 1974.

Cornwall, J. M.: Cyclotron instabilities and electromagnetic emission in the ultra-low frequency and very low frequency ranges, J. Geophys. Res., 70, 61–69, https://doi.org/10.1029/JZ070i001p00061, 1965.

Erlandson, R. E., Aggson, T. L., Hogey, W. R., and Slavin, J. A.: Simultaneous observations of subauroral electron temperature enhancements and electromagnetic ion cyclotron waves, Geophys. Res. Lett., 20, 1723–1726, https://doi.org/10.1029/93gl01975, 1993.

Gary, S. P. and Lee, M. A.: The ion cyclotron anisotropy instability and the inverse correlation between proton anisotropy and proton beta, J. Geophys. Res. Space Phys., 99, 11297–11302, https://doi.org/10.1029/94JA00253, 1994.

Gary, S. P. and Wang, J.: Whistler instability: Electron anisotropy upper bound, *J. Geophys. Res. Space Phys.*, 101, 10749–10754, https://doi.org/10.1029/96JA00326, 1996.

Hellberg, M. A. and Mace, R. L.: Generalized plasma dispersion function for a plasma with a kappa-Maxwellian velocity distribution, Phys. Plasmas, 9, 1495–1504, https://doi.org/10.1063/1.1462636, 2002.

Hellinger, P. and Matsumoto, H.: New kinetic instability: Oblique Alfvén fire hose, J. Geophys. Res. Space Phys., 105, 10519–10526, https://doi.org/10.1029/1999JA000297, 2000.

Kennel, C. F. and Petschek, H. E.: Limit on stably trapped particle fluxes, J. Geophys. Res., 71, 1–28, https://doi.org/10.1029/JZ071i001p00001, 1966.

Klimas, A. J., Vassiliadis, D., and Baker, D. N.: Dst index prediction using data-derived analogues of the magnetospheric dynamics, J. Geophys. Res. Space Phys., 103, 20435–20447, https://doi.org/10.1029/98JA01559, 1998.

Kozyra, J. U., Shelley, E. G., Comfort, R. H., Brace, L. H., Cravens, T. E., and Nagy, A. F.: The role of ring current O+ in the formation of stable auroral red arcs, J. Geophys. Res., 92, 7487–7502, https://doi.org/10.1029/JA092iA07p07487, 1987.

Lazar, M. and Schlickeiser, R.: Covariant kinetic theory for nonlinear plasma waves interaction, J. Plasma Phys., 72, 711–720, https://doi.org/10.1017/S0022377805004253, 2006.

Lazar, M., Schlickeiser, R., and Shukla, P. K.: Cumulative effect of the filamentation and Weibel instabilities in counterstreaming thermal plasmas, Phys. Plasmas, 13, 102107, https://doi.org/10.1063/1.2357047, 2006.

Livadiotis, G.: Kappa Distributions: Theory and Applications in Plasmas, Elsevier, 1st Edn., 380 pp., ISBN 9780128046388, 2017.

Lazar, M.: The electromagnetic ion-cyclotron instability in bi-Kappa distributed plasmas, Astron. Astrophys., 547, A94, https://doi.org/10.1051/0004-6361/201219861, 2012.

Ma, Q., Li, W., Yue, C., Thorne, R. M., Bortnik, J., Kletzing, C. A., Kurth, W. S., Hospodarsky, G. B., Reeves, G. D., and Spence, H. E.: Ion Heating by Electromagnetic Ion Cyclotron Waves and Magnetosonic Waves in the Earth's Inner Magnetosphere, Geophys. Res. Lett., 46, 6258–6267, https://doi.org/10.1029/2019GL083513, 2019.

Meda, R. and Ahirwar, G.: Effect of kappa distribution function on EMIC waves in cold magnetized plasma by particle aspect analysis, J. Emerg. Technol. Innov. Res., 8(8), 410, https://www.jetir.org, 2021.

Omura, Y., Pickett, J., Grison, B., Santolik, O., Dandouras, I., Engebretson, M., Decreau, PierretteP. M. E., and Masson, A.: Theory and observation of electromagnetic ion cyclotron triggered emissions in the magnetosphere, J. Geophys. Res., 115, A07234, https://doi.org/10.1029/2010JA015300, 2010.

Patel, S., Varma, P., and Tiwari, M. S.: Electromagnetic ion cyclotron waves in multi-ions hot anisotropic plasma in auroral acceleration region-particle aspect approach, Earth Moon Planets, 109, 29–41, https://doi.org/10.1007/s11038-012-9400-4, 2012.

Pierrard, V. and Lazar, M.: Kappa Distributions: Theory and Applications in Space Plasmas, Sol. Phys., 267, 153–174, https://doi.org/10.1007/s11207-010-9640-2, 2010.

Sugiyama, H., Singh, S., Omura, Y., Shoji, M., Nunn, D., and Summers, D.: Electromagnetic ion cyclotron waves in the Earth's magnetosphere with a kappa-Maxwellian particle distribution, J. Geophys. Res. Space Phys., 120, 8426–8439, https://doi.org/10.1002/2015JA021346, 2015.

Summers, D. and Thorne, R. M.: The modified plasma dispersion function, Phys. Fluids B Plasma Phys., 3(7), 1835–1847, https://doi.org/10.1063/1.859653, 1991.

Usanova M. E., Drozdov A., Orlova K., Mann I. R., Shprits Y., Robertson M. T., Turner D. L., Milling D. K., Kale A., Baker D. N., Thaller S. A., Reeves G. D., Spence H. E., Kletzing C., Wygant J.:Effect of EMIC waves on relativistic and ultrarelativistic electron populations: Ground-based and Van Allen Probes observations, *Geophys. Res. Lett.*, **41**, 1375–1381, https://doi.org/10.1002/2013GL059024, 2014.

573   Vasyliunas, V. M.: Survey of low-energy electrons in the evening sector of the magnetosphere
574   with OGO 1 and OGO 3, J. Geophys. Res., 73(9), 2839, https://doi.org/10.1029/JA073i009p02839,
575   1968.

576   Xiao, F., Zhou, Q., He, H., Zheng, H., and Wang, S.: Electromagnetic ion cyclotron waves
577   instability threshold condition of suprathermal protons by kappa distribution, J. Geophys. Res., 112,
578   A07219, https://doi.org/10.1029/2006JA012050, 2007.

579   Xue, S., Thorne, R. M., and Summers, D.: Electromagnetic ion-cyclotron instability in space
580   plasmas, J. Geophys. Res., 98(A10), 17475–17484, https://doi.org/10.1029/93JA00790, 1993.

581   Xue, S., Thorne, R. M., and Summers, D.: Growth and damping of oblique electromagnetic ion
582   cyclotron waves in the Earth's magnetosphere, J. Geophys. Res., 101(A7), 15457–15466,
583   https://doi.org/10.1029/96JA01088, 1996 a.

584   Xue, S., Thorne, R. M., and Summers, D.: Parametric study of electromagnetic ion cyclotron
585   instability in the Earth's magnetosphere, J. Geophys. Res. Space Phys., 101(A7), 15467–15474,
586   https://doi.org/10.1029/96JA01087, 1996 b.

587   Yan, G., Shen, C., Liu, Z., and others: Solar wind transport into the magnetosphere caused by
588   magnetic reconnection at high latitude magnetopause during northward IMF: Cluster-DSP conjunction
589   observations, Sci. China Ser. E Technol. Sci., 51, 1677–1684, https://doi.org/10.1007/s11431-008-
590   0260-0, 2008.